



MIT Open Access Articles

Enhancement of Thermoelectric Performance of n-Type PbSe by Cr Doping with Optimized Carrier Concentration

The MIT Faculty has made this article openly available. **Please share** how this access benefits you. Your story matters.

Citation	Zhang, Qian, Eyob Kebede Chere, Kenneth McEnaney, Mengliang Yao, Feng Cao, Yizhou Ni, Shuo Chen, Cyril Opeil, Gang Chen, and Zhifeng Ren. "Enhancement of Thermoelectric Performance of n-Type PbSe by Cr Doping with Optimized Carrier Concentration." <i>Adv. Energy Mater.</i> 5, no. 8 (January 7, 2015): n/a–n/a.
As Published	http://dx.doi.org/10.1002/aenm.201401977
Publisher	Wiley Blackwell
Version	Author's final manuscript
Citable link	http://hdl.handle.net/1721.1/99761
Terms of Use	Creative Commons Attribution-Noncommercial-Share Alike
Detailed Terms	http://creativecommons.org/licenses/by-nc-sa/4.0/

Enhancement of Thermoelectric Performance of n-type PbSe by Cr Doping with Optimized Carrier Concentration

Qian Zhang,^{a,†} Eyob Kebede Chere,^{a,†} Kenneth McEnaney,^b Mengliang Yao,^c Feng Cao,^a Yizhou Ni,^a Shuo Chen,^a Cyril Opeil,^c Gang Chen,^b and Zhifeng Ren^{a*}

ABSTRACT: Ti, V, Cr, Nb, and Mo were found to be effective in increasing the Seebeck coefficient and power factor of n-type PbSe at temperature below 600 K. We found that the higher Seebeck coefficients and power factors are due to higher Hall mobility $\sim 1000 \text{ cm}^2 \text{ V}^{-1} \text{ s}^{-1}$ at lower carrier concentration. A larger average ZT value (relevant for applications) can be obtained by an optimization of carrier concentration to $\sim 10^{18}$ - 10^{19} cm^{-3} . Even though the highest room temperature power factor $\sim 3.3 \times 10^{-3} \text{ W m}^{-1} \text{ K}^{-2}$ is found in 1 at. % Mo-doped PbSe, the highest ZT is achieved in Cr-doped PbSe. Combined with the lower thermal conductivity, ZT was improved to ~ 0.4 at room temperature and peak ZT s of ~ 1.0 were observed at $\sim 573 \text{ K}$ for $\text{Pb}_{0.9925}\text{Cr}_{0.0075}\text{Se}$ and $\sim 673 \text{ K}$ for $\text{Pb}_{0.995}\text{Cr}_{0.005}\text{Se}$. The calculated device efficiency of $\text{Pb}_{0.995}\text{Cr}_{0.005}\text{Se}$ is as high as $\sim 12.5\%$ with cold side 300 K and hot side 873 K, higher than those of all the n-type PbSe materials reported in literature.

^aDepartment of Physics and TcSUH, University of Houston, Houston, Texas 77204, USA

Email: zren@uh.edu

^bDepartment of Mechanical Engineering, Massachusetts Institute of Technology, Cambridge, Massachusetts 02139, USA

^cDepartment of Physics, Boston College, Chestnut Hill, Massachusetts 02467, USA

Q.Z., and E.-K.C. contributed equally.

INTRODUCTION

Lead chalcogenide thermoelectric (TE) materials have been drawing increased attention for their high maximum dimensionless figures of merit $ZT = [S^2\sigma/(\kappa_L+\kappa_e)]T$, where S is the Seebeck coefficient, σ the electrical conductivity, κ_L the lattice thermal conductivity, κ_e the electronic thermal conductivity, and T the absolute temperature.¹⁻⁶ However, high TE device efficiency (η) depends on the high average ZT of the TE material over the temperature range, $\eta_{\max} = [(T_H-T_C)/T_H] [(1+ZT_{\text{average}})^{1/2}-1]/[(1+ZT_{\text{average}})^{1/2}+T_C/T_H]$, where T_H is the temperature at the hot junction and T_C the temperature at the cold junction,⁷⁻¹¹ Combining in series different materials with different peak ZT temperatures may boost the TE device efficiency,¹²⁻¹⁶ but suffers from the added complexity of bonding, interfacial mass diffusion, and thermal expansion mismatch. It is therefore preferable to use a single material to span the whole temperature range of operation. In the case of lead chalcogenides, peak ZT s normally appear at around 673-873 K.¹⁻⁶ The ZT curve increases steeply from room temperature to the peak ZT temperature, resulting in relatively low average ZT , especially for PbSe.^{17, 18} Through the combination of nanostructures and complex band structure, an increased average ZT was obtained in Na-doped p-type PbTe/Ag₂Te (300-750 K)¹⁹ compared with pure Na-doped PbTe²⁰ and La-doped n-type PbTe/Ag₂Te.²¹ An increase in average ZT was also achieved in Na-doped Pb_{0.97}Mg_{0.03}Te (300-750 K) due to the stabilization of the optimal carrier concentration.²² In comparison, PbSe is attractive as it is cheaper, but its average ZT needs to be further improved. Among all reported n- and p-type PbSe,^{4, 17, 18, 23-26} Al-doped n-type PbSe has the highest average ZT , which may be due to nanostructures that reduce thermal conductivity and resonant states that improved the Seebeck coefficient.²⁶ The resonant states could be responsible for the boosted Seebeck coefficient, power factor and ZT at lower temperatures. It was reported that Cr is effective in increasing the Seebeck coefficient and power factor of PbTe with, however, no resonant effect from the Cr-formed deep resonant level, which is 100 meV above the conduction band bottom of PbTe.²⁷⁻³¹ A similar deep resonant level was also found in Cr-doped PbSe with energy 124 meV above the conduction band bottom of PbSe.³² The similar enhanced Seebeck coefficient and power factor, together with the lower thermal conductivity compared with PbTe-based materials contributed to the higher efficiency in Cr-doped PbSe. Although the application of any lead-based materials for

thermoelectric devices and systems in different regions of the world is controversial, it still attracted a great attention due to the higher ZT s that might lead to higher conversion efficiency.

In this paper, we systematically present different doped n-type PbSe (Ti-,³³⁻³⁵ V-, Cr-, Nb- and Mo-doped PbSe) with enhanced power factors and ZT s (below 600 K), especially for Cr-doped PbSe, which also has a peak $ZT > 1$, promising to have a potential device efficiency ~12.5% for a cold side of 300 K and a hot side 873 K for $\text{Pb}_{0.995}\text{Cr}_{0.005}\text{Se}$, higher than those of all other reported n-type PbSe thermoelectric materials.^{4, 17, 18, 23-26}

EXPERIMENTAL SECTION

We prepared n-type PbSe with different doping elements $\text{Pb}_{1-x}\text{A}_x\text{Se}$ (A: Ti, V, Cr, Nb, and Mo, $x \leq 0.02$) by melting, hand milling, and hot pressing. The raw materials with nominal compositions were sealed in the carbon coated quartz tube and slowly (200 °C/h) raised to 1100 °C and kept for 6 h, then slowly (200 °C/h) cooled to 650 °C and stayed at that temperature for 50 h, finally slowly (200 °C/h) cooled to room temperature. The obtained ingots were cleaned and hand milled in a glove box. The powder was loaded into the half-inch die and hot pressed by direct current (dc-HP) press at 600 °C for 2 min under pressure of 80 MPa.^{4, 18} X-ray diffraction spectra analysis was conducted on a PANalytical multipurpose diffractometer with an X'celerator detector (PANalytical X'Pert Pro). The microstructures were investigated by a scanning electron microscope (SEM, JEOL 6330F) and a high resolution transmission electron microscope (HRTEM, JEOL 2100F). The chemical composition was analyzed on an energy-dispersive X-ray (EDX) spectrometer attached to TEM. The electrical resistivity (ρ) and Seebeck coefficient (S) were simultaneously measured on a commercial system (ULVAC ZEM-3). The thermal conductivity κ was calculated using $\kappa = D\alpha C_p$, where D is volumetric density determined by the Archimedes method, α the thermal diffusivity obtained on a laser flash apparatus (Netzsch LFA 457), and C_p the specific heat measured on a differential scanning calorimetry thermal analyzer (Netzsch DSC 404 C). The Hall Coefficient R_H at room temperature was measured using a PPMS (Quantum Design Physical Properties Measurement System). The Hall carrier concentration n_H and Hall mobility μ_H were calculated using $n_H = 1/(eR_H)$ and $\mu_H = \sigma R_H$, respectively. The uncertainty for the electrical conductivity is 3%, the Seebeck coefficient 5%, the thermal conductivity 7% (comprising uncertainties of 4% for the thermal diffusivity, 5% for the specific heat, and 3% for the density), so the combined

uncertainty for the power factor is 10% and that for ZT value is 12%. Error bars were not used in the figures to increase the readability of the curves.

RESULTS AND DISCUSSION

Single phase $\text{Pb}_{1-x}\text{Cr}_x\text{Se}$ was obtained with different Cr doping concentrations ($x = 0.0025, 0.005, 0.0075, \text{ and } 0.01$), which is indexed to the face-centered structure (space group $\text{Fm}\bar{3}\text{m}$) and shown in figure 1. Due to the difference between the ionic radius of Pb^{2+} (1.20 Å) and Cr^{3+} (0.52 Å), the lattice parameter decreased with increasing x (see Table 1). Even though secondary phases $\text{Cr}_{3+\delta}\text{Te}_4$ and Cr_2Te_3 were observed when PbTe was doped with more than 0.4 at. % Cr,³⁰ no impurity formed in Cr-doped PbSe even up to 1 at. %.

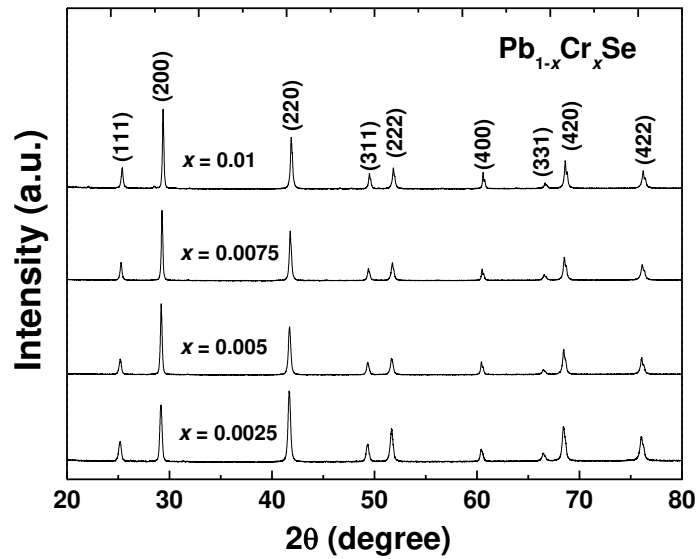


Fig. 1 XRD patterns for $\text{Pb}_{1-x}\text{Cr}_x\text{Se}$ ($x = 0.0025, 0.005, 0.0075, \text{ and } 0.01$).

Tab 1. The lattice parameters and the densities of $\text{Pb}_{1-x}\text{Cr}_x\text{Se}$ ($x = 0.0025, 0.005, 0.0075, \text{ and } 0.01$).

Nominal composition	$\text{Pb}_{0.9975}\text{Cr}_{0.0025}\text{Se}$	$\text{Pb}_{0.995}\text{Cr}_{0.005}\text{Se}$	$\text{Pb}_{0.9925}\text{Cr}_{0.0075}\text{Se}$	$\text{Pb}_{0.99}\text{Cr}_{0.01}\text{Se}$
Lattice parameter (Å)	6.126	6.122	6.118	6.112
Density (g cm^{-3})	8.1	8.05	7.98	8

Normally, lead chalcogenides are favorable for hot side temperatures at 673-873 K. $(\text{Bi}_{1-x}\text{Sb}_x)_2(\text{Te}_{1-y}\text{Se}_y)_3$ is usually considered over the temperature range from 300 to 473 K. Therefore, a combination of $(\text{Bi}_{1-x}\text{Sb}_x)_2(\text{Te}_{1-y}\text{Se}_y)_3$ with mid to high temperature TE materials will yield a higher device efficiency across a large temperature range. However, we found also good TE properties in PbSe based materials from 300 to 473 K when Cr was doped into PbSe to enable higher average ZT across a large temperature range (300-873 K). Figure 2 (a-f) presents the temperature dependence of electrical conductivity, Seebeck coefficient, power factor, thermal diffusivity, specific heat, total thermal conductivity and lattice thermal conductivity for $\text{Pb}_{1-x}\text{Cr}_x\text{Se}$ ($x = 0.0025, 0.005, 0.0075, \text{ and } 0.01$) compared with reported data on n-type $\text{Bi}_2\text{Te}_{2.7}\text{Se}_{0.3}$.³⁶ All the samples show metallic transport behavior. The electrical conductivity is higher than $\text{Bi}_2\text{Te}_{2.7}\text{Se}_{0.3}$, and the Seebeck coefficient is comparable with $\text{Bi}_2\text{Te}_{2.7}\text{Se}_{0.3}$ below 473 K. The room temperature power factor reaches $\sim 3.0 \times 10^{-3} \text{ W m}^{-1} \text{ K}^{-2}$, higher than all the reported doped PbSe and even $\text{Bi}_2\text{Te}_{2.7}\text{Se}_{0.3}$.^{4, 17, 18, 23-26, 36} Even though a high room temperature power factor of $\sim 3.849 \times 10^{-3} \text{ W m}^{-1} \text{ K}^{-2}$ was reported in the 1.45 at. % Cr-doped PbTe sample,²⁸ the overall ZT is not favorable due to the high thermal conductivity. PbSe has been shown to have lower lattice thermal conductivity than PbTe, which has been attributed to the higher degree of anharmonicity of lattice vibrations in PbSe.¹⁷ The lattice thermal conductivity of Cr-doped PbSe was calculated by subtracting the charge carrier thermal conductivity from total thermal conductivity ($\kappa_L = \kappa_{\text{total}} - \kappa_e = \kappa_{\text{total}} - L\sigma T$, where L is the Lorenz number calculated using a two-band model¹⁸) and given in figure 2 (f). It is even lower than In doped PbSe below 700 K.¹⁸ In figure 3, we show the representative SEM (a), low magnification TEM (b) and HRTEM (c), (d) images for $\text{Pb}_{0.995}\text{Cr}_{0.005}\text{Se}$. The sample consists of both big grains with several to several tens of micrometers (Fig. 3 (a)) and small grains with several tens to hundreds of nanometers (Fig. 3 (b)) and dislocations both on grain boundaries (Fig. 3 (c)) and within the grains (Fig. 3 (d)), which is in agreement with the observation in the similar system.^{37, 38} All these are supposed to contribute to the effective phonon scattering for the lower lattice thermal conductivity. Combined with this relatively lower thermal conductivity, the room temperature ZT reaches ~ 0.4 (shown in figure 4), much higher than the previous In-doped n-type PbSe¹⁸, although it is still lower than the room temperature ZT of $\text{Bi}_2\text{Te}_{2.7}\text{Se}_{0.3}$.³⁶ The ZT values continuously increase and reach ~ 1.0 at ~ 573 K for $\text{Pb}_{0.9925}\text{Cr}_{0.0075}\text{Se}$ and ~ 673 K for $\text{Pb}_{0.995}\text{Cr}_{0.005}\text{Se}$ and stay above 0.9 from 573 K to 873 K, which strongly increases the average ZT of the PbSe based materials, as will be discussed later.

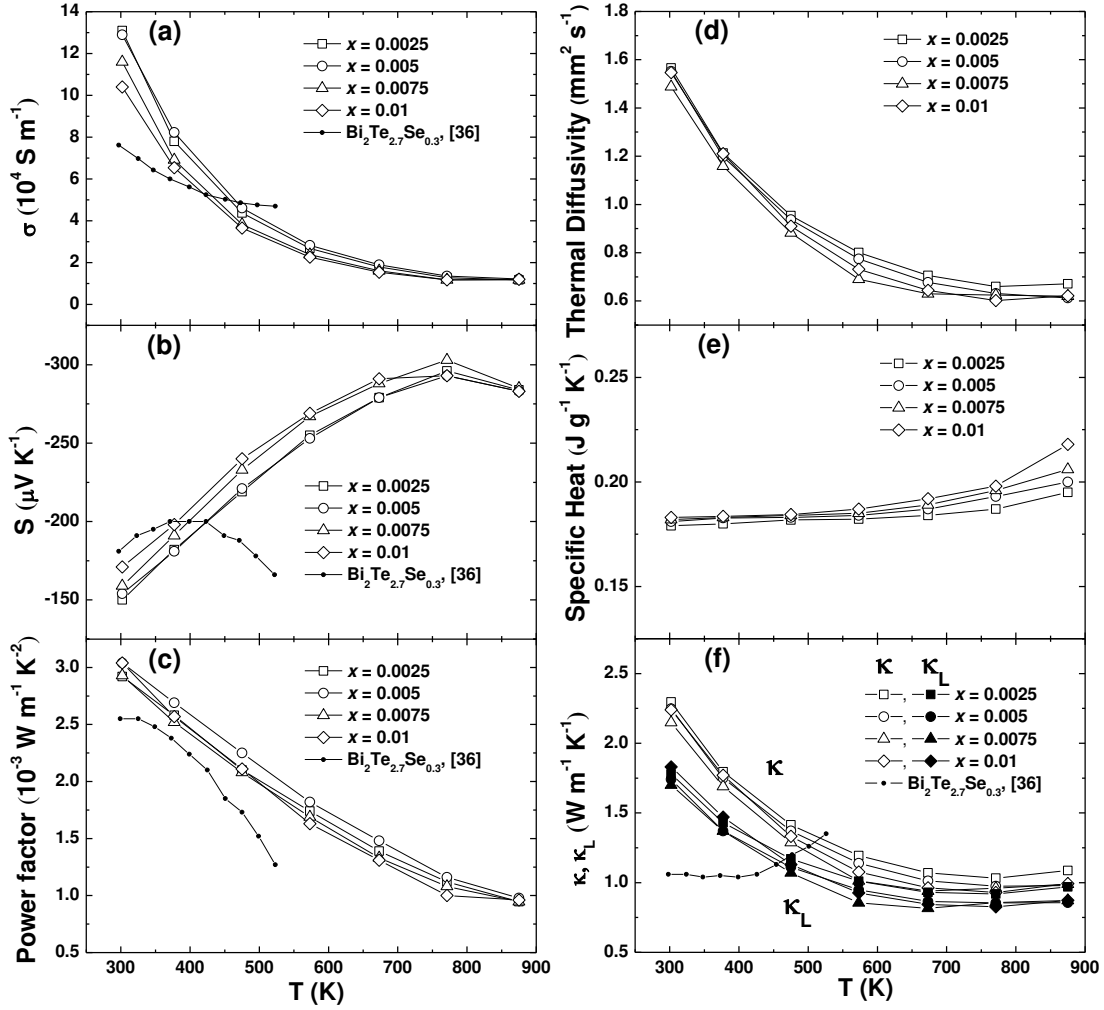


Fig. 2 Temperature dependence of (a) electrical conductivity, (b) Seebeck coefficient, (c) power factor, (d) thermal diffusivity, (e) specific heat and (f) total thermal conductivity and lattice thermal conductivity for $\text{Pb}_{1-x}\text{Cr}_x\text{Se}$ ($x = 0.0025, 0.005, 0.0075, \text{ and } 0.01$) in comparison with reported data on n-type $\text{Bi}_2\text{Te}_{2.7}\text{Se}_{0.3}$ by Yan *et al.*³⁶ (small solid circles).

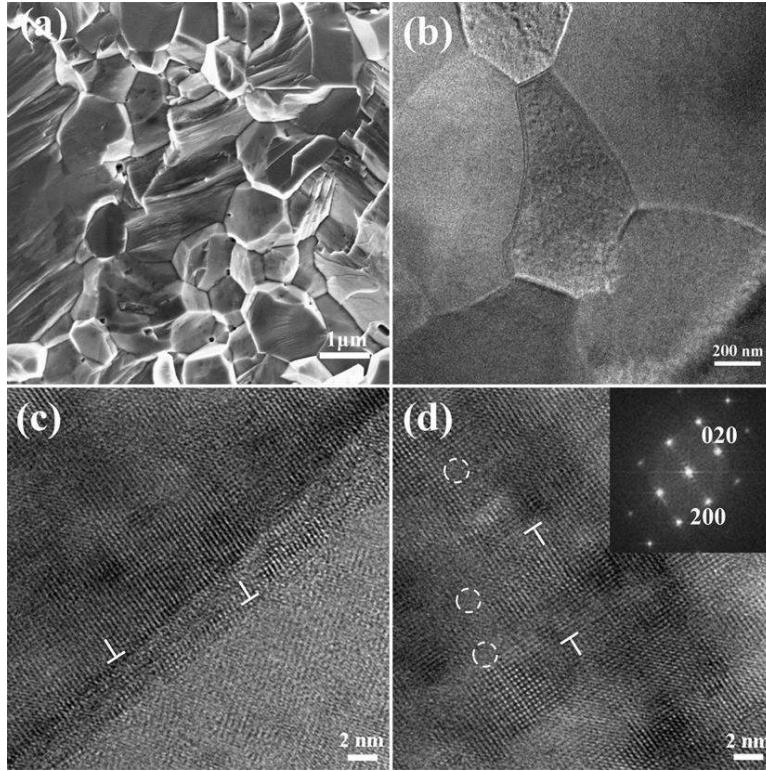


Fig. 3 Representative SEM image (a) of $\text{Pb}_{0.995}\text{Cr}_{0.005}\text{Se}$. Low magnification TEM image (b), HRTEM images (c) showing a grain boundary, and (d) an individual grain, inset: the corresponding diffraction pattern along [011] direction, showing a single crystal. Some thread dislocations are marked by \perp , and point defects by dotted circles in (c) and (d).

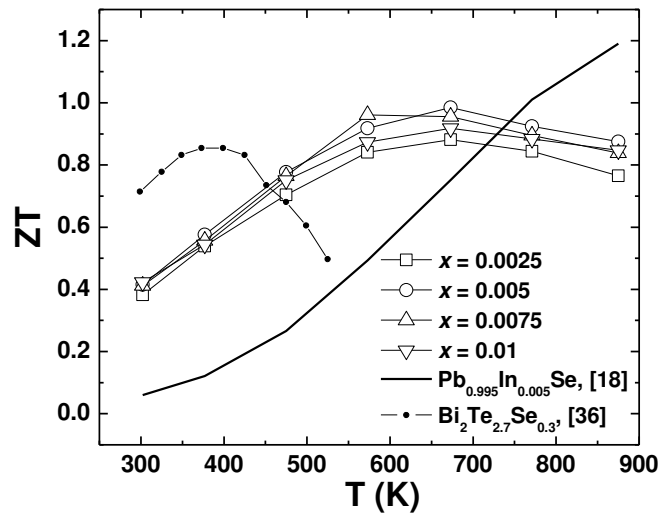


Fig. 4 Temperature dependence of ZT for $\text{Pb}_{1-x}\text{Cr}_x\text{Se}$ ($x = 0.0025, 0.005, 0.0075, \text{ and } 0.01$) in comparison with reported data on $\text{Bi}_2\text{Te}_{2.7}\text{Se}_{0.3}$ by Yan *et al.*³⁶ (small solid circles) and our previous data on In-doped PbSe ¹⁸ (black line).

Following the method outlined above for Cr-doped PbSe , we also doped other transition metals close to Cr (in the periodic table of elements) into PbSe . The temperature dependence of the electrical conductivity, Seebeck coefficient, power factor, thermal diffusivity, specific heat, total thermal conductivity, and lattice thermal conductivity for optimized $\text{Pb}_{1-x}\text{A}_x\text{Se}$ (A: Ti, V, Cr, Nb, and Mo) ($x = 0.005$ or 0.01) in comparison with reported data on In-doped PbSe ¹⁸ (solid line) are shown in figure 5. The samples still show the typical behavior of degenerate semiconductors. It is interesting that the TE properties of all the transition metal-doped PbSe show a consistent trend, but different from the previous two categories doping (like Ga-, In-, and Br-, Cl-doped PbSe ^{18, 24, 25}). The electrical conductivity of the transition metal-doped PbSe is lower and the Seebeck coefficient is good across the whole temperature range (300–873 K). The power factor decreased with increasing temperature. The highest room temperature power factor is $\sim 3.3 \times 10^{-3} \text{ W m}^{-1} \text{ K}^{-2}$ for 1 at. % Mo-doped PbSe . According to the microstructures of all the transition metal-doped PbSe in figure 3 and figure S1. The higher lattice thermal conductivity of V-doped PbSe is due to the absence of small size grains (see figure S1b). However, because of the lower electronic contribution to thermal conductivity, the total thermal conductivity of all the transition metal-doped PbSe is lower than that of In-doped PbSe ¹⁸. With a lower thermal conductivity and a higher power factor at lower temperatures, the ZT values of all the studied samples are higher than In-doped PbSe ¹⁸ below 600 K (shown in figure 6). The highest room temperature ZT is ~ 0.5 for 1 at. % Mo-doped PbSe and the highest peak ZT is ~ 1.0 for 0.5 at. % Cr-doped PbSe at about 673 K.

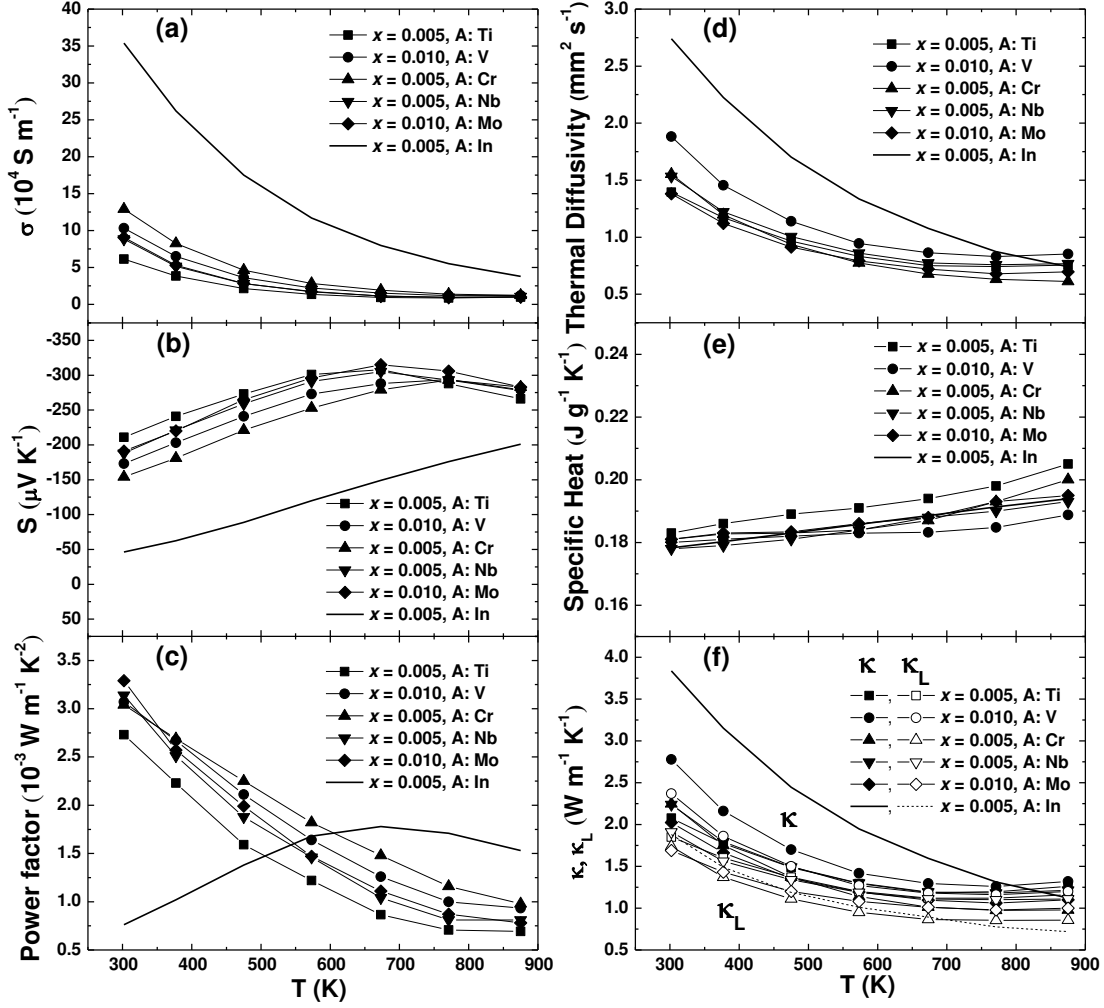


Fig. 5 Temperature dependence of (a) electrical conductivity, (b) Seebeck coefficient, (c) power factor, (d) thermal diffusivity, (e) specific heat, and (f) total thermal conductivity and lattice thermal conductivity for optimized $\text{Pb}_{1-x}\text{A}_x\text{Se}$ (A: Ti, V, Cr, Nb, and Mo) ($x = 0.005$ or 0.01) in comparison with previously reported data on $\text{Pb}_{1-x}\text{In}_x\text{Se}$ ($x = 0.005$)¹⁸ (solid line).

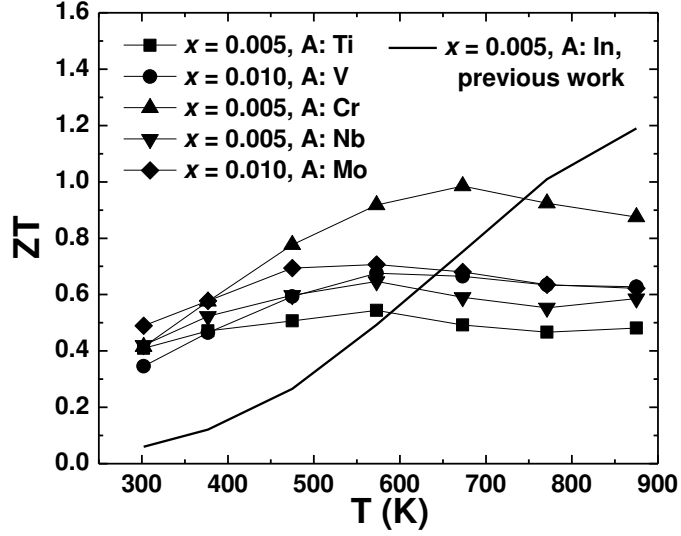


Fig. 6 Temperature dependence of ZT for $Pb_{1-x}A_xSe$ (A: Ti, V, Cr, Nb, and Mo) ($x = 0.005$ or 0.01) in comparison with reported data on $Pb_{1-x}In_xSe$ ($x = 0.005$)¹⁸ (solid line).

What is the reason for these attractive room temperature power factors? In figure 7, we summarize the room temperature Pisarenko relations for $Pb_{1-x}A_xSe$ (A: Ti, V, Nb, and Mo) ($x = 0.005$ or 0.01) and $Pb_{1-x}Cr_xSe$ ($x = 0.0025, 0.005, 0.0075,$ and 0.01) (open squares) in this work in comparison with all the reported n-type $PbSe$.^{18, 24-26} Considering the nonparabolicity of the conduction band of $PbSe$, a two-band Kane (TBK) model was used to fit the data. The Cl- and Br-doped $PbSe$ are fitted well with an effective mass of $m^* = 0.27 m_e$ (dashed line)^{24,25} and B-, Ga- and In-doped $PbSe$ with $m^* = 0.5 m_e$ (solid line)¹⁸. Due to the resonant scattering, Al-doped $PbSe$ deviates from the fitting line, showing almost constant Seebeck coefficient with increasing carrier concentration.²⁶ Similar with B-, Ga- and In-doped $PbSe$, all the transition metal Ti-, V-, Cr-, Nb-, and Mo-doped $PbSe$ fell onto the fitting line with effective mass $m^* = 0.5 m_e$. In spite of the formed deep resonant level in Cr-doped $PbSe$,³² there is no effect of resonant scattering at all, nor is there in any of the other (Ti, V, Nb and Mo) transition metal-doped $PbSe$ materials. Also the room temperature relationships between μ and n for the optimal transition metal-doped $PbSe$, together with all the reported n-type $PbSe$ are shown in figure 8.^{18, 24-26} Only Al-doped $PbSe$ deviates largely due to resonant scattering.²⁶ Actually the present higher Seebeck coefficient is mostly attributed to the lower carrier concentration, which is in the range of $(4-10) \times 10^{18} \text{ cm}^{-3}$. To compare our data, we included most of the room temperature properties for

optimally n-type doped PbSe by Ti, V, Cr, Nb, and Mo; B, Al, Ga, and In; Cl and Br in table 2. The higher room temperature ZT is mainly related to the higher room temperature power factor ($PF = S^2 n \mu q$). Both Seebeck coefficient (S) and Hall mobility (μ) are inversely proportional to Hall carrier concentration (n) (see figure 7 and figure 8). With relatively low n , the transition metal-doped PbSe has both higher S and μ , contributing to the higher power factor at room temperature (also see figure S2 (a)). We usually optimize the Hall carrier concentration to $\sim 10^{19}$ - 10^{20} cm^{-3} for high peak ZT . However, it seems that the optimal Hall carrier concentration is $\sim 10^{18}$ - 10^{19} cm^{-3} for good ZT at room temperature, so it is possible to get the ideal average ZT by balancing the Hall carrier concentration. Certainly, the carrier concentration is not the only parameter (see figure S2 (b)), we must also consider the other parameters, such as Hall mobility, effective mass, lattice thermal conductivity, *etc.*, which all together determines the higher average ZT in Cr-doped PbSe.

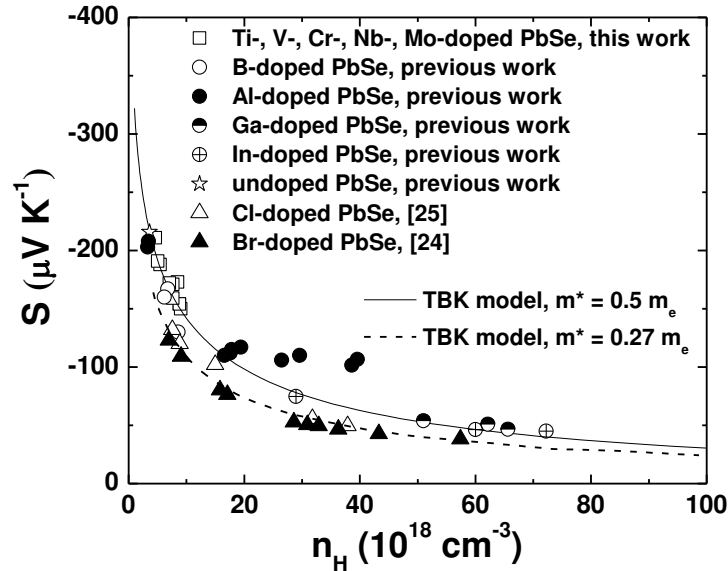


Fig. 7 Room temperature Pisarenko plots for $\text{Pb}_{1-x}\text{A}_x\text{Se}$ (A: Ti, V, Nb, and Mo) ($x = 0.005$ or 0.01) and $\text{Pb}_{1-x}\text{Cr}_x\text{Se}$ ($x = 0.0025, 0.005, 0.0075,$ and 0.01) (open squares) in comparison with reported data on B-doped PbSe (open circles), Al-doped PbSe (solid circles), Ga-doped PbSe (half open circles), In-doped PbSe (plus in circles) and undoped PbSe (open stars) in our previous work,^{18, 26} and Cl-doped PbSe by Androulakis *et al.* (open triangles)²⁴ and Br-doped PbSe by Wang *et al.* (solid triangles).²⁵ Black curve is based on nonparabolic two-band Kane

model (TBK) with the electron effective mass of PbSe $m^* = 0.5 m_e$.¹⁸ Dashed curve is based on nonparabolic TBK with the electron effective mass of PbSe $m^* = 0.27 m_e$.²⁵

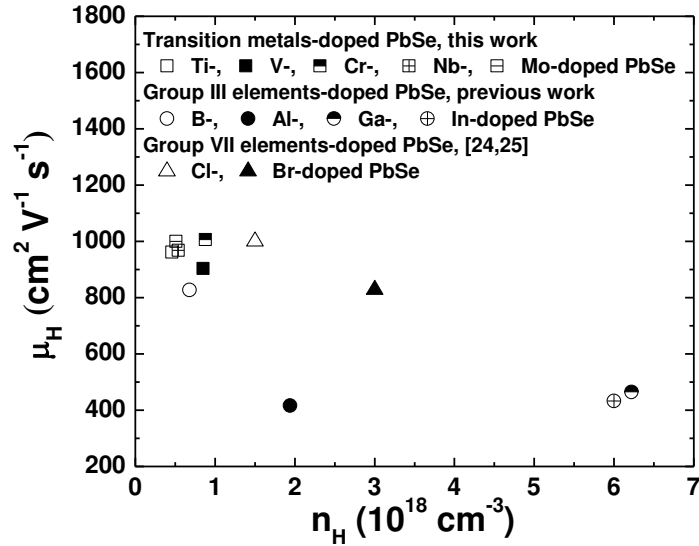


Fig. 8 Room temperature relationships between Hall μ and Hall n for transition metals-doped PbSe: $\text{Pb}_{0.995}\text{Ti}_{0.005}\text{Se}$, (open squares) $\text{Pb}_{0.99}\text{V}_{0.01}\text{Se}$ (solid squares), $\text{Pb}_{0.995}\text{Cr}_{0.005}\text{Se}$ (half open squares), $\text{Pb}_{0.995}\text{Nb}_{0.005}\text{Se}$ (plus in squares), and $\text{Pb}_{0.99}\text{Mo}_{0.01}\text{Se}$ (minus in squares) in comparison with reported data on PbSe doped with group III elements: $\text{Pb}_{0.98}\text{B}_{0.02}\text{Se}$ (open circles), $\text{Pb}_{0.99}\text{Al}_{0.01}\text{Se}$ (solid circles), $\text{Pb}_{0.995}\text{Ga}_{0.005}\text{Se}$ (half open circles), and $\text{Pb}_{0.995}\text{In}_{0.005}\text{Se}$ (plus in circles) [18, 26], and PbSe doped with group VII elements: $\text{PbSe}_{0.996}\text{Cl}_{0.004}$ (open triangles) [24], and $\text{Pb}_{1.002}\text{Se}_{0.9982}\text{Br}_{0.0018}$ (solid triangles) [25]. The data of Al-doped PbSe (solid circle) deviates largely due to the resonant scattering.

Tab. 2 Comparison of room temperature properties for optimally doped n-type PbSe by Ti, V, Cr, Nb, and Mo; B¹⁸, Al²⁶, Ga¹⁸, and In¹⁸; Cl²⁴ and Br²⁵.

Comp.	Density (g cm ⁻³)	σ (10 ⁴ S m ⁻¹)	S ($\mu\text{V K}^{-1}$)	PF (10 ⁻³ W m ⁻¹ K ⁻²)	n_{H} (10 ¹⁹ cm ⁻³)	μ (cm ² V ⁻¹ s ⁻¹)	κ_{total} (W m ⁻¹ K ⁻¹)	κ_{L} (W m ⁻¹ K ⁻¹)	ZT
$\text{Pb}_{0.995}\text{Ti}_{0.005}\text{Se}$	8.14	6.13	-211	2.73	0.46	962	2.077	1.85	0.41
$\text{Pb}_{0.99}\text{V}_{0.01}\text{Se}$	8.20	10.3	-173	3.07	0.85	904	2.078	2.37	0.35
$\text{Pb}_{0.995}\text{Cr}_{0.005}\text{Se}$	8.05	12.9	-154	3.04	0.88	1006	2.247	1.74	0.42
$\text{Pb}_{0.995}\text{Nb}_{0.005}\text{Se}$	8.20	8.84	-188	3.14	0.54	968	2.239	1.91	0.42
$\text{Pb}_{0.99}\text{Mo}_{0.01}\text{Se}$	8.10	9.05	-191	3.29	0.51	1000	2.025	1.69	0.49
$\text{Pb}_{0.98}\text{B}_{0.02}\text{Se}$	7.87	8.72	-167	2.42	0.68	827	2.119	1.79	0.34

Pb _{0.99} Al _{0.01} Se	7.90	12.9	-117	1.17	1.94	416	2.280	1.34	0.23
Pb _{0.995} Ga _{0.005} Se	7.94	38.5	-51	1	6.22	465	3.759	1.69	0.08
Pb _{0.995} In _{0.005} Se	7.9	35.4	-46.4	0.76	6	433	3.838	1.86	0.06
PbSe _{0.996} Cl _{0.004}	8.02	~23	~-105	~-2.53	1.5	~1000	~-2.67	~-1.9	~-0.27
Pb _{1.002} Se _{0.9982} Br _{0.0018}	>8.1	~48.6	-52	~-1.31	3	~828	~-3.38	~-1.28	~-0.11

The discretization method of Mahan was used to estimate the device efficiency of the legs made by some of the n-type PbSe (solid lines) and n-type Bi₂Te_{2.7}Se_{0.3} (dashed line) with the cold side temperature at 300 K.³⁹⁻⁴² We assumed the heat flow in the leg to be one-dimensional, neglecting losses from the side walls of the leg.¹³

$$\frac{dT}{dx} = \frac{JST-Q}{\kappa} \quad (1)$$

$$\frac{dQ}{dx} = \rho J^2 + JS \frac{dT}{dx} \quad (2)$$

$$\frac{dV}{dx} = -\rho J - S \frac{dT}{dx} \quad (3)$$

Where J , Q , ρ , V , S , κ , and T are the current density, heat flux density, electrical resistivity, voltage, Seebeck coefficient, thermal conductivity and temperature, respectively. The leg efficiency is calculated from the output power and input heat flux into the leg by:

$$\eta_{leg} = \frac{J(V_c - V_h)}{Q_h} \quad (4)$$

The results are shown in figure 9. Cr-doped PbSe has the highest efficiency for a wide range of hot-side temperatures (350-873 K), even though higher peak ZT s are achieved in other n-type PbSe materials (1.3 at 850 K for Al doped PbSe,²⁶ 1.2 at 850 K for Br-doped PbSe,²⁵ and 1.2 at 873 K for Ga-, In-doped PbSe¹⁸ compared to only 1.0 at 673 K for Cr-doped PbSe). At the lower temperature range, when the hot side temperature is between 350 K and 523 K, the device efficiency of Cr-doped PbSe is only slightly lower than that of the temperature-limited n-type Bi₂Te_{2.7}Se_{0.3}.³⁶ At high hot-side temperatures, the efficiency of Cr-doped PbSe is only rivaled by Al-doped PbSe, a material which has much lower efficiency at lower hot-side temperatures. These results emphasize the benefits of a flatter ZT curve: not only is the efficiency higher at high temperatures, but also the efficiency is higher at a wide range of hot-side temperatures.

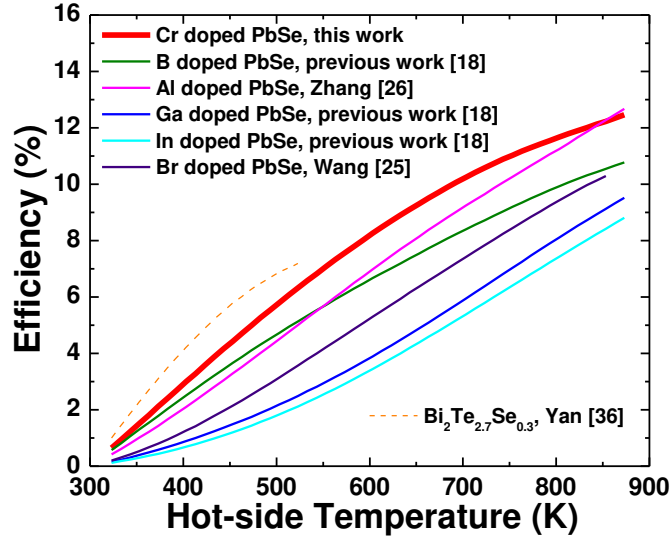


Fig. 9 Temperature dependence of device efficiency for 0.5 at. % Cr doped PbSe (this work, red) in comparison with the optimized B-doped PbSe (green),¹⁸ Al-doped PbSe (pink),²⁶ Ga-doped PbSe (blue),¹⁸ In-doped PbSe (light blue),¹⁸ Br-doped PbSe (purple),²⁵ and Bi₂Te_{2.7}Se_{0.3} (dashed orange)³⁶ with cold side temperature 300 K.

Instead of the comparison of the peak ZT s, we present average ZT s (integrating of the area below the ZT curves) from 300 to 873 K (Fig. 10a, left panel) and device ZT s (obtained from the theoretically calculated power efficiency) operated between 300 K and 873 K (Fig. 10b, left panel) for some of the n-type PbSe materials. We also present the average ZT s between 300 K and 523 K (Fig. 10a, right panel) and device ZT s operated between 300 K and 523 K (Fig. 10b, right panel) for some n-type PbSe materials compared with n-type Bi₂Te_{2.7}Se_{0.3}. Cr-doped PbSe has both a preferred average ZT and a device ZT compared to the other n-type PbSe, especially when working between 300 K and 523 K, but not as good as Bi₂Te_{2.7}Se_{0.3}. Furthermore, the device ZT of Cr-doped PbSe (between 300 K and 873 K) is even higher than that of the reported n-type PbTe:La/Ag₂Te (between 300 K and 775 K) which has a peak ZT of ~ 1.6 at 775 K.²¹ Many of the best p-type PbTe materials, such as PbTe:Na (between 300 K and 750 K) with peak $ZT \sim 1.4$ at about 750 K,²⁰ PbTe:Tl (between 300 K and 775 K) with peak $ZT \sim 1.4$ at about 775 K,¹ PbTe:Na/SrTe (between 300 K and 775 K) with peak $ZT \sim 1.5$ at about 775 K,⁴³ and PbTe_{0.85}Se_{0.15}:Na (between 300 K and 800 K) with peak $ZT \sim 1.8$ at about 800 K,³ could benefit from a flatter ZT curve. Considering the cost of Se compared to Te, and the higher device efficiency and wider working temperature range of PbSe than PbTe, PbSe has the potential to

replace PbTe for thermoelectric applications. Also the multiple repeated tests show good thermal stability of this material (Figure S3 and S4), which enables the potential applications. More work is expected in increasing the device efficiency of p-type PbSe.

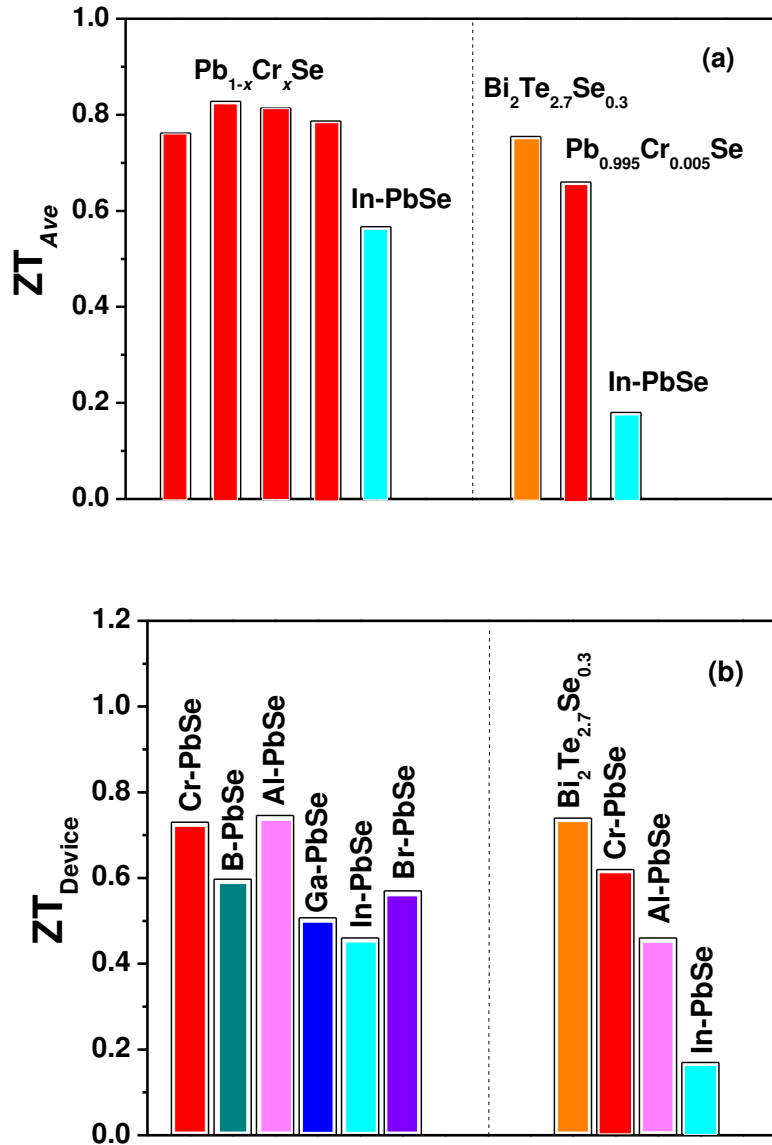


Fig. 10 (a) Comparison of average ZT from 300 K to 873 K between $Pb_{1-x}Cr_xSe$ ($x = 0.0025, 0.005, 0.0075, \text{ and } 0.01$) (this work, red) and optimized In-doped PbSe (light blue) (left panel)¹⁸. Comparison of average ZT from 300 K to 523 K for $Bi_2Te_{2.7}Se_{0.3}$ (orange)³⁶, 0.5 at. % Cr doped PbSe (this work, red) and optimized In-doped PbSe (light blue) (right panel)¹⁸. (b) Comparison

of device ZT operated between 300 K and 873 K for 0.5 at. % Cr-doped PbSe (this work, red) and optimized B- (green),¹⁸ Al- (pink),²⁶ Ga- (blue),¹⁸ In- (light blue)¹⁸, and Br- (purple)²⁵ doped PbSe (left panel). Comparison of device ZT operated between 300 K and 523 K for Bi₂Te_{2.7}Se_{0.3} (orange),³⁶ 0.5 at. % Cr-doped PbSe (this work, red) and optimized Al- (pink),²⁶ In-doped PbSe (light blue)¹⁸ (right panel).

CONCLUSIONS

Transition metals (Ti, V, Cr, Nb, and Mo) can enhance the lower temperature (below 600 K) TE properties of n-type PbSe. Specifically, Cr doping in PbSe increases the room temperature ZT to ~ 0.4 and the peak ZT to ~ 1.0 between 573 K and 673 K, hence increasing the average ZT and efficiency of n-type PbSe over a wide temperature range (300 K to 873 K). This boost is not attributed to a resonant states effect. The optimal Hall carrier concentration is $\sim 10^{18}$ - 10^{19} cm⁻³ for good average ZT in Cr-doped PbSe. By further tuning the carrier concentration, even better properties can be expected. Cr-doped n-type PbSe is believed to be promising for power generation applications.

ACKNOWLEDGEMENT: This work is supported by “Solid State Solar Thermal Energy Conversion Center (S³TEC)”, an Energy Frontier Research Center funded by the U.S. Department of Energy, Office of Science, Office of Basic Energy Science under award number DE-SC0001299.

REFERENCES

- 1 J. P. Heremans, V. Jovovic, E. S. Toberer, A. Saramat, K. Kurosaki, A. Charoenphakdee, S. Yamanaka, G. J. Snyder, *Science* **2008**, 321, 554.
- 2 A. D. LaLonde, Y. Z. Pei, G. J. Snyder, *Energy Environ. Sci.* **2011**, 4, 2090.
- 3 Y. Z. Pei, X. Y. Shi, A. LaLonde, H. Wang, L. D. Chen, G. J. Snyder, *Nature* **2011**, 473, 66.

- 4 Q. Zhang, F. Cao, W. S. Liu, K. Lukas, B. Yu, S. Chen, C. Opeil, G. Chen, Z. F. Ren, *J. Am. Chem. Soc.* **2012**, *134*, 10031.
- 5 Q. Y. Zhang, H. Z. Wang, Q. Zhang, W. S. Liu, B. Yu, H. Wang, D. Z. Wang, G. Ni, G. Chen, Z. F. Ren, *Nano Lett.* **2012**, *12*, 2324.
- 6 R. J. Korkosz, T. C. Chasapis, S. Lo, J. W. Y. J. Kim, C. Wu, E. Hatzikraniotis, T. P. Hogan, D. N. Seidman, C. Wolverton, V. P. Dravid, M. G. Kanatzidis, *J. Am. Chem. Soc.* **2014**, *136*, 3225.
- 7 D. M. Rowe, *CRC Handbook of Thermoelectrics, Macro to Nano*; CRC Press, Taylor & Francis Group, Boca Raton, **2006**.
- 8 B. Poudel, Q. Hao, Y. Ma, Y. Lan, A. Minnich, B. Yu, X. Yan, D. Wang, A. Muto, D. Vashaee, X. Chen, J. Liu, M. S. Dresselhaus, G. Chen, Z. F. Ren, *Science* **2008**, *320*, 634.
- 9 D. Kraemer, B. Poudel, H. P. Feng, J. C. Caylor, B. Yu, X. Yan, Y. Ma, X. W. Wang, D. Z. Wang, A. Muto, K. McEnaney, M. Chiesa, Z. F. Ren, G. Chen, *Nature Mater.* **2011**, *10*, 532.
- 10 L. P. Hu, T. J. Zhu, Y. G. Wang, H. H. Xie, Z. J. Xu, X. B. Zhao, *NPG Asia Mater.* **2014**, *6*, e88.
- 11 F. Cao, K. McEnaney, G. Chen, Z. F. Ren, *Energy Environ. Sci.* **2014**, *7*, 1615.
- 12 G. H. Zeng, J. H. Bahk, J. E. Bowers, H. Lu, A. C. Gossard, S. L. Singer, A. Majumdar, Z. X. Bian, M. Zebarjadi, A. Shakouri, *Appl. Phys. Lett.* **2009**, *95*, 083503.
- 13 W. S. Liu, K. Lukas, K. McEnaney, S. Lee, Q. Zhang, C. Opeil, G. Chen, Z. F. Ren, *Energy Environ. Sci.* **2013**, *6*, 552.
- 14 C. Hadjistassou, E. Kyriakides, J. Georgiou, *Energ. Convers. Manage.* **2013**, *66*, 165.
- 15 S. Yoon, J. Y. Cho, H. Koo, S. H. Bae, S. Ahn, G. R. Kim, J. S. Kim, C. Park, *J. Elec. Mater.* **2014**, *43*, 414.
- 16 P. H. Ngan, D. V. Christensen, G. J. Snyder, L. T. Hung, S. Linderoth, N. V. Nong, N. Pryds, *Phys. Status Solidi A*, **2014**, *211*, 9.
- 17 H. Wang, Y. Pei, A. D. LaLonde, G. J. Snyder, *Adv. Mater.* **2011**, *23*, 1366.
- 18 Q. Zhang, F. Cao, K. Lucas, W. S. Liu, K. Esfarjani, C. Opeil, D. Broido, D. Parker, D. J. Singh, G. Chen, Z. F. Ren, *J. Am. Chem. Soc.* **2012**, *134*, 17731.
- 19 Y. Z. Pei, A. H. Nicholas, A. LaLonde, G. J. Snyder, *Energy Environ. Sci.* **2011**, *4*, 3640.
- 20 Y. Pei, A. LaLonde, S. Iwanaga, G. J. Snyder, *Energy Environ. Sci.* **2011**, *4*, 2085.

- 21 Y. Pei, J. Lensch-Falk, E. S. Toberer, D. L. Medlin, G. J. Snyder, *Adv. Funct. Mater.* **2011**, *21*, 241.
- 22 Y. Z. Pei, A. D. LaLonde, N. A. Heinz, X. Y. Shi, S. Iwanaga, H. Wang, L. D. Chen, G. J. Snyder, *Adv. Mater.* **2011**, *23*, 5674.
- 23 G. T. Alekseeva, E. A. Gurieva, P. P. Konstantinov, L. V. Prokof'eva, M. I. Fedorov, *Semicond.* **1996**, *30*, 1125.
- 24 J. Androulakis, D. Y. Chung, X. L. Su, L. Zhang, C. Uher, M. G. Kanatzidis, *Phys. Rev. B* **2011**, *84*, 155207.
- 25 H. Wang, Y. Z. Pei, A. D. LaLonde, G. J. Snyder, *Proc. Natl. Acad. Sci. USA.* **2012**, *109*, 9705.
- 26 Q. Y. Zhang, H. Wang, W. S. Liu, H. Z. Wang, B. Yu, Q. Zhang, Z. T. Tian, G. Ni, S. Lee, K. Esfarjani, G. Chen, Z. F. Ren, *Energy Environ. Sci.* **2012**, *5*, 5246.
- 27 M. I. Baleva, L. D. Borissova, *J. Phys. C: Solid State Phys.* **1983**, *16*, L907.
- 28 B. Paul, P. Banerji, *J. Appl. Phys.* **2011**, *109*, 103710.
- 29 B. Paul, P. K. Rawat, P. Banerji, *Appl. Phys. Lett.* **2011**, *98*, 262101.
- 30 M. D. Nielsen, E. M. Levin, C. M. Jaworski, K. Schmidt-Rohr, J. P. Heremans, *Phys. Rev. B* **2012**, *85*, 045210.
- 31 E. P. Skipetrov, N. A. Pichugin, E. I. Slyn'ko, V. E. Slyn'ko, *Semiconductors* **2013**, *47*, 729.
- 32 T. Story, Z. Wilamowski, E. Grodzicka, D. Dobrowolski, B. Witkowska, *Acta Phys. Polonica A* **1995**, *87*, 229.
- 33 F. F. Sizov, V. V. Teterkin, L. V. Prokof'eva, E. A. Gurieva, *Sov. Phys. Semicond.* **1980**, *14*, 1063.
- 34 V. V. Teterkin, F. F. Sizov, L. V. Prokofeva, Y. S. Gromovoi, M. N. Vinogradova, *Sov. Phys. Semicond.* **1983**, *17*, 489.
- 35 J. D. König, M. D. Nielsen, Y. B. Gao, M. Winkler, A. Jacquot, H. Böttner, J. P. Heremans, *Phys. Rev. B* **2011**, *84*, 205126.
- 36 X. Yan, B. Poudel, Y. Ma, W. S. Liu, G. Joshi, H. Wang, Y. C. Lan, D. Z. Wang, G. Chen, Z. F. Ren, *Nano Lett.* **2010**, *10*, 3373.
- 37 Q. Zhang, Y. C. Lan, S. L. Yang, F. Cao, M. L. Yao, C. Opeil, D. Broido, G. Chen, Z. F. Ren, *Nano Energy* **2013**, *2*, 1121.

- 38 H. Z. Wang, Q. Y. Zhang, B. Yu, H. Wang, W. S. Liu, G. Chen, Z. F. Ren, *J. Mater. Res.* **2011**, *26*, 912.
- 39 G. D. Mahan, *J. Appl. Phys.* **1991**, *70*, 4551.
- 40 J. Snyder, T. S. Ursell, *Phys. Rev. Lett.* **2003**, *91*, 148021.
- 41 H. J. Goldsmid, *Introduction to thermoelectricity*, Springer-Verlag, Berlin Heidelberg, **2010**.
- 42 A. Muto, J. Yang, B. Poudel, Z. F. Ren, G. Chen, *Adv. Energy Mater.* **2013**, *3*, 245.
- 43 K. Biswas, J. He, Q. Zhang, G. Wang, C. Uher, V. P. Dravid, M. G. Kanatzidis, *Nat. Chem.* **2011**, *3*, 160.